

# *Theoretical Predictions of the Interfacial Stress Transfer in Nanotube-Reinforced Polymer Nanocomposites by Using a Strain-Hardening Shear-Lag Model*

**Feilin Gou & Changhong Ke**

**Multiscale Science and Engineering**

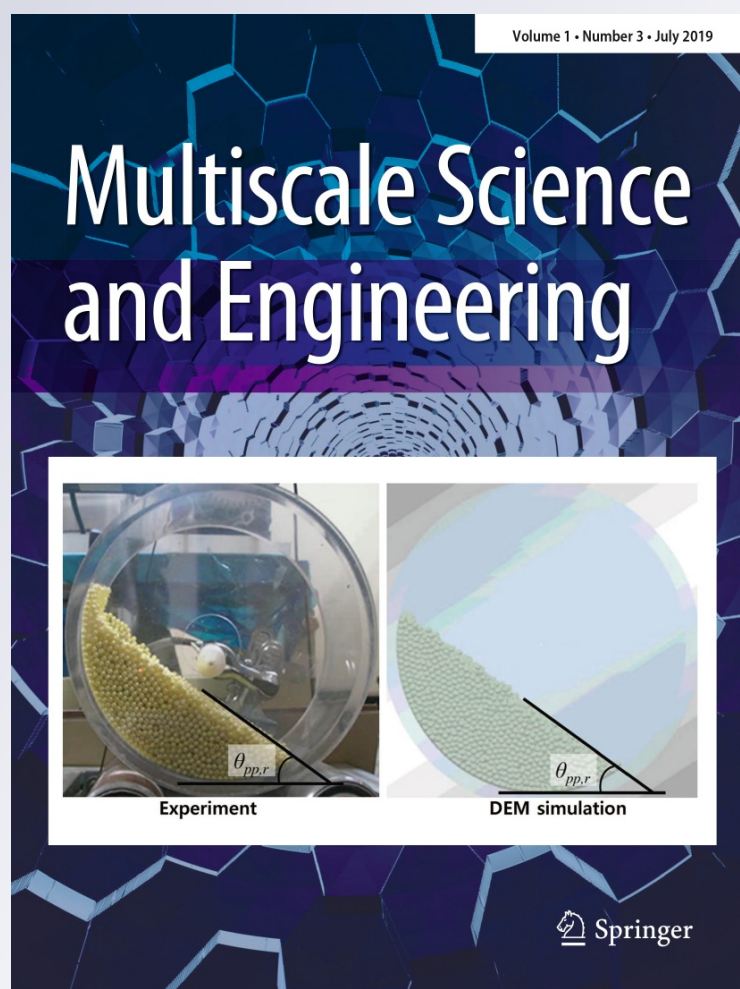
ISSN 2524-4515

Volume 1

Number 3

Multiscale Sci. Eng. (2019) 1:236-246

DOI 10.1007/s42493-019-00021-5



**Your article is protected by copyright and all rights are held exclusively by Korean Multi-Scale Mechanics (KMSM). This e-offprint is for personal use only and shall not be self-archived in electronic repositories. If you wish to self-archive your article, please use the accepted manuscript version for posting on your own website. You may further deposit the accepted manuscript version in any repository, provided it is only made publicly available 12 months after official publication or later and provided acknowledgement is given to the original source of publication and a link is inserted to the published article on Springer's website. The link must be accompanied by the following text: "The final publication is available at [link.springer.com](http://link.springer.com)".**



# Theoretical Predictions of the Interfacial Stress Transfer in Nanotube-Reinforced Polymer Nanocomposites by Using a Strain-Hardening Shear-Lag Model

Feilin Gou<sup>1</sup> · Changhong Ke<sup>1,2</sup> 

Received: 17 February 2019 / Revised: 25 April 2019 / Accepted: 23 May 2019 / Published online: 5 June 2019  
© Korean Multi-Scale Mechanics (KMSM) 2019

## Abstract

Interfacial load transfer inside nanofiber-reinforced polymer nanocomposites plays a vital role in capitalizing on the extraordinary mechanical properties of the added nanofibers and in governing their bulk mechanical performance. In this paper, we investigate the load transfer characteristics of nanotube–polymer interfaces by using a micromechanics shear-lag model that takes into account the elastoplastic properties of polymer matrices. Closed-form analytical solutions of the interfacial shear stress distribution profile are derived. The failure of the nanotube–polymer interface and the pull-out force are analyzed using this model based on recently reported nanomechanical single-nanotube pull-out experiments that were conducted on carbon nanotube and boron nitride nanotube polymer interfaces. The theoretical predictions are in good agreement with experimental measurements. The findings from this work are useful to a better understanding of the interfacial load transfer characteristics of nanofiber-reinforced polymer nanocomposites and ultimately contribute to the optimal design and performance of lightweight and high-strength nanocomposite materials. The presented micromechanics model and the analytical solutions can be extended to study the interfacial stress transfer inside 1D nanofiber-reinforced metal and ceramic nanocomposites as well as of 2D material based composites and devices.

**Keywords** Interfacial load transfer · Nanotubes · Pull-out tests · Polymer nanocomposites · Shear-lag model

## Introduction

Fiber-reinforced polymer nanocomposites are promising engineering materials for a number of industries (e.g., the aerospace and automotive industries) because of their light, strong and durable characteristics. Carbon nanotubes (CNTs) [1] and boron nitride nanotubes (BNNTs) [2, 3] are two types of one-dimensional (1D) tubular nanostructures with many exceptional structural and physical (mechanical, thermal, chemical and so on) properties and are widely considered to be ideal reinforcing additives for lightweight and high-strength polymer nanocomposites [4–7]. The enhanced bulk properties of fiber-reinforced polymer nanocomposites

critically rely on effective load transfer on fiber–polymer interfaces [8–10], which is essential to capitalize on the extraordinary mechanical properties of the added nanofibers. However, despite many advances in the past two decades, the scientific understanding of the interfacial load transfer on nanotube–polymer interfaces remains as one of the most significant technical challenges in the full realization of the reinforcing potentials of the added nanotubes. Single-nanotube pull-out measurements are ideal small-scale experimental techniques to study the nanotube–polymer interface and have revealed quantitatively the interfacial load carrying capacity and the dependences of the interfacial strength on the embedded nanotube length and diameter as well as a matrix's material properties [7, 11–21]. These direct and quantitative measurements represent significant scientific advances as compared with the qualitative and indirect assessments from bulk measurements [22, 23]. However, the localized stress transfer properties of the nanotube–polymer interface, such as the distribution profile of the interfacial shear stress (IFSS) and the maximum interfacial shear strength, remain inaccessible to experiments and have to rely

✉ Changhong Ke  
cke@binghamton.edu

<sup>1</sup> Department of Mechanical Engineering, State University of New York at Binghamton, Binghamton, NY 13902, USA

<sup>2</sup> Materials Science and Engineering Program, State University of New York at Binghamton, Binghamton, NY 13902, USA

on theoretical modeling and computational simulations for quantification [24].

In single-nanotube pull-out measurements, a single nanotube that is partially embedded inside a matrix is stretched by an increasing tensile force that is applied to the free end of the nanotube and eventually pulled out of the matrix. During the pulling process, a non-uniform point-wise IFSS distribution along the entire nanotube–matrix interface occurs. The IFSS possesses its maximum value at the nanotube's entry position into the matrix and decays towards the nanotube's embedded end. Therefore, interface failure initiates at the nanotube entry position. Subsequently, the initiated crack propagates through the entire nanotube–matrix interface, resulting in a complete de-bonding between nanotube and matrix. The maximum IFSS upon interface failure is an intrinsic material property that indicates the bonding strength of the nanotube–matrix interaction and is substantially higher than the average IFSS, which is defined by assuming a uniform distribution of the shear stress along the entire nanotube–matrix interface. During the nanotube stretching process, the matrix material that is in direct contact with the nanotube surface may deform elastically or plastically. The IFSS distribution in fiber-reinforced composites has been investigated by using shear-lag models [25–29]. By assuming a linear elastic deformation in a matrix, the analytical solutions of the IFSS distribution reported by Jiang and Penn [30] have been widely employed in the interpretation of the single-nanofiber/nanotube pull-out measurements and to the quantification of the maximum IFSS [7, 11–21, 31]. The elastic matrix deformation assumption implies that the maximum IFSS should be lower than the matrix's yield shear stress. However, some of the reported values for the maximum IFSS of nanotube–polymer interfaces have substantially exceeded the yield shear stress of the employed polymer matrices. For example, the maximum IFSS of the interfaces formed by CNTs with poly(methyl methacrylate) (PMMA) is reported to reach about 155 MPa [19], which is substantially higher than the reported yield shear stress of PMMA (about 22–65 MPa) in the literature [32–38]. Similarly, the maximum IFSS of the interfaces formed by BNNTs with epoxy is reported to be about 323 MPa [7], which is more than one order of magnitude higher than the yield shear stress of the employed epoxy (about 20 MPa based on the manufacturer data [39]). The much higher reported values of the maximum IFSS indicate that substantial plastic deformations may occur in the matrix, in particular in those regions adjacent to the nanotube surface and at or near the nanotube's entry position. The negligence of the yielding deformation of the matrix in the shear-lag model inevitably leads to an over-estimation of the maximum IFSS. This is because the matrix, under an elastic deformation assumption, would become much stiffer at relatively large strains (i.e., over the elastic strain limit) and

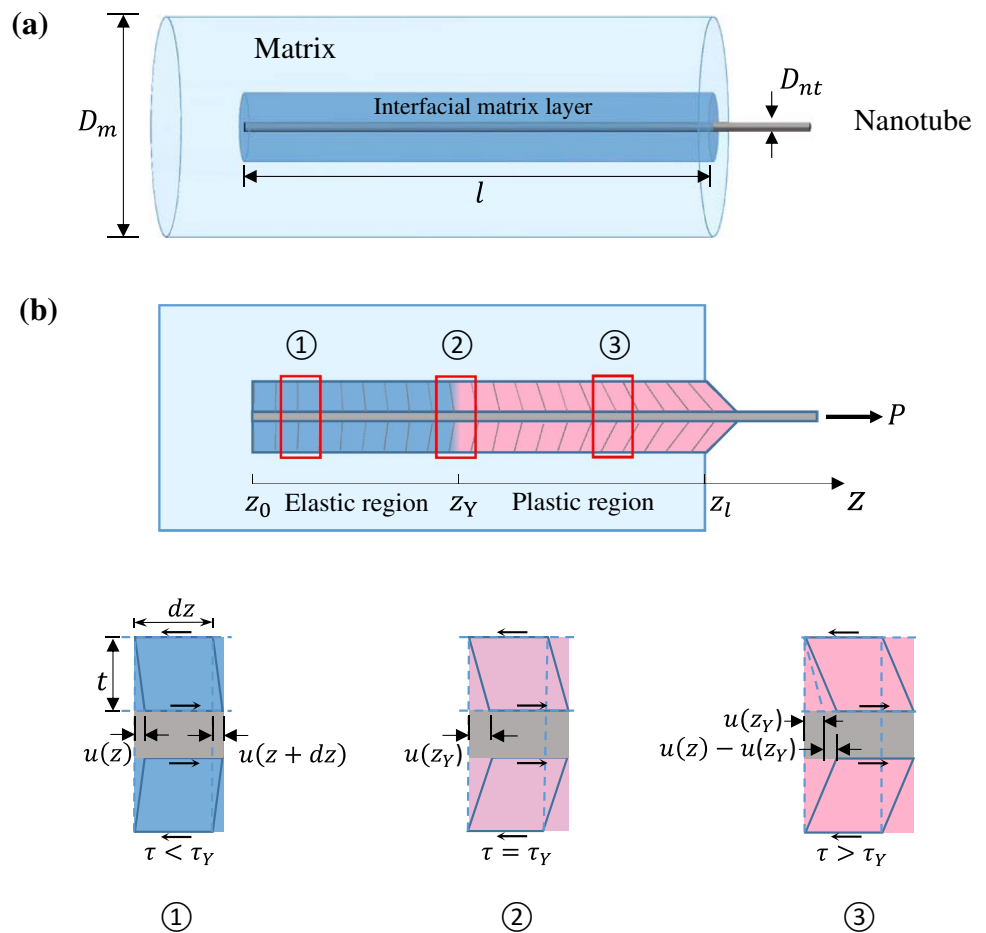
thus store more strain energies in the region adjacent to the nanotube entry position. Therefore, it is essential to consider the matrix's yielding in the shear-lag model to ensure a more realistic and accurate interpretation of the single-nanotube pull-out measurements and for a better understanding of the load transfer characteristics of nanotube–polymer interfaces. Here, we present a micromechanics model to describe the shear-lag effect on the load transfer characteristics of the nanotube–polymer interface by taking into account the elastoplastic (or strain hardening) behaviors of polymer matrices. We use this model to analyze the recently reported single-nanotube pull-out experiments that were conducted on the respective interfaces formed by CNTs and BNNTs with PMMA and epoxy [7, 19, 21].

## Results and Discussion

### Formulation of the Strain-Hardening Shear-Lag Continuum Mechanics Model and Closed-Form Analytical Solutions

Figure 1a, b illustrate the undeformed and deformed configurations of a single nanotube composite, respectively, which are schematically identical to the testing schemes employed in the nanomechanical single-nanotube pull-out measurements [7, 19, 21]. In the configurations, a straight nanotube of an outer diameter  $D_{nt}$  is partially embedded in a matrix with an embedded length of  $l$ . For simplicity, the matrix volume that encloses the partially embedded nanotube is assumed to be a concentric cylinder with a diameter  $D_m$ . A uniform and continuous interface is assumed between the embedded nanotube surface and the surrounding matrix. When an axial stretching force is applied to the protruding nanotube as illustrated in Fig. 1b, the entire nanotube is stretched along the force direction, which results in the deformation of the matrix adjacent to the interface area via the shear force on the nanotube–matrix interface. Here, the matrix deformation is assumed to occur only in the region in a close proximity to the nanotube surface, which is denoted here as an interfacial matrix layer. The interfacial matrix layer is a hollow cylinder with a thickness of  $t$  and is under pure shear deformations. The shear deformation of the interfacial matrix layer can be generally divided into two segments: the elastic region ( $z_0 \leq z < z_Y$ ) and the plastic region ( $z_Y \leq z \leq z_l$ ), where  $z$  is the coordinate axis along the nanotube's longitudinal direction,  $z_0$  is the position of the nanotube's embedded end,  $z_l$  is the nanotube entry position, and  $z_Y$  indicates the onset location of matrix yielding. In this model, the nanotube is considered to be a purely elastic material, while the matrix is a bilinear elastoplastic material. The interfacial shear stress,  $\tau_i$ , is assumed to be in a

**Fig. 1** Schematic illustration of the strain-hardening shear-lag model. **a** The initial undeformed 3D nanotube/matrix configuration. The hollow cylinder region (dark-blue) that encloses the outer nanotube surface is the interfacial matrix layer. **b** The deformed nanotube/matrix configuration. The pure shear deformations in the interfacial matrix layer are visualized with the aid of the added short mesh lines and colors (blue: elastic deformation; pink: plastic deformation). The free-body diagrams at the bottom illustrate elements in the elastic, onset of yielding, and plastic regions



linear relationship with the nanotube displacement  $u(z)$  and is given as,

$$\tau_i = \begin{cases} K_1 \cdot u(z), & z_0 \leq z < z_Y \\ K_2 \cdot [u(z) - u(z_Y)] + \tau_Y, & z_Y \leq z \leq z_l \end{cases} \quad (1)$$

where  $\tau_Y$  is the yield shear stress of matrix;  $K_1 = \frac{G^m}{t}$  and  $K_2 = \frac{G_p^m}{t}$ , in which  $G^m$  and  $G_p^m$  are the shear modulus of the matrix before and after yielding, respectively. It is noted that  $G_p^m$  can be derived by using  $J_2$ -deformation theory in pure shear condition [40] and is given as  $\frac{1}{G_p^m} = \frac{1}{G^m} + \frac{3}{E_p^m} - \frac{3}{E^m}$ , where  $E_p^m$  is the tangent modulus of the matrix after yielding. For quasi-static loading conditions, the total shear force on the nanotube–matrix interface equals the external stretching force  $P$ , i.e.,  $\pi \int_{z_0}^{z_l} \tau_i \cdot D_{nt} dz = P$ .

The equilibrium equation for the nanotube along its longitudinal direction is given as

$$\sigma_z \cdot D_{nt} - 4 \int_{z_0}^z \tau_i dz = 0, \quad (2)$$

where  $\sigma_z$  is the normal stress in the nanotube and is given as

$$\sigma_z = E^{nt} \frac{du(z)}{dz}, \quad (3)$$

where  $E^{nt}$  is the Young's modulus of nanotubes.

By inserting Eqs. (1) and (3) into Eq. (2), we get

$$D_{nt} \cdot E^{nt} \frac{d^2 u(z)}{dz^2} - 4K_1 u(z) = 0, \quad z_0 \leq z < z_Y, \quad (4a)$$

$$D_{nt} \cdot E^{nt} \frac{d^2 u(z)}{dz^2} - 4K_2 [u(z) - u(z_Y)] - 4\tau_Y = 0, \quad z_Y \leq z \leq z_l. \quad (4b)$$

The general solution of Eq. (4a) is given as

$$u(z) = C_1 e^{\sqrt{D} \cdot z} + C_2 e^{-\sqrt{D} \cdot z}, \quad (5)$$

where  $D = \frac{4K_1}{D_{nt} \times E^{nt}}$ , and  $C_1$  and  $C_2$  are two constants to be determined from the boundary conditions. The boundary conditions for the elastic deformation region are  $\sigma_z = 0$  at  $z = 0$  and  $u(z) = \frac{\tau_Y}{K_1}$  at  $z = z_Y$ . By applying the boundary conditions to Eq. (5), we get

$$C_1 = C_2 = \frac{u(z_Y)}{e^{\sqrt{D} \cdot z_Y} + e^{-\sqrt{D} \cdot z_Y}}. \quad (6)$$

The normal stress in the nanotube at  $z = z_Y$  is given as,

$$\sigma_z(z_Y) = E^{nt} C_1 \sqrt{D} \left( e^{\sqrt{D} \cdot z_Y} - e^{-\sqrt{D} \cdot z_Y} \right). \tag{7}$$

The general solution of Eq. (4b) is given as

$$u(z) = C_3 e^{\sqrt{A} \cdot z} + C_4 e^{-\sqrt{A} \cdot z} + \frac{B}{A}, \tag{8}$$

where  $A = \frac{4K_2}{D_m \times E^m}$ ,  $B = \frac{4[K_2 u(z_Y) - \tau_Y]}{D_m \times E^m}$ , and  $C_3$  and  $C_4$  are two constants to be determined from the boundary conditions. The boundary conditions for the plastic deformation region are  $u(z_Y) = \frac{\tau_Y}{K_1}$  and the known value of the normal stress  $\sigma_z(z_Y)$  that is given by Eq. (7). Applying the boundary conditions to Eq. (8), we get

$$C_3 = \left( \frac{\sigma_z(z_Y)}{2E^{nt} \sqrt{A}} - \frac{B}{2A} + \frac{\tau_Y}{2K_1} \right) e^{-\sqrt{A} \cdot z_Y}, \tag{9}$$

$$C_4 = \left( -\frac{\sigma_z(z_Y)}{2E^{nt} \sqrt{A}} - \frac{B}{2A} + \frac{\tau_Y}{2K_1} \right) e^{\sqrt{A} \cdot z_Y}. \tag{10}$$

Substituting Eqs. (5), (6), (8), (9), and (10) into Eqs. (1) and (3) leads to the solutions of the normal stress in the nanotube and the IFSS on the nanotube–matrix interface, which are given as,

$$\sigma_z(z) = \begin{cases} \frac{\sqrt{D} E^{nt} u(z_Y)}{e^{\sqrt{D} \cdot z_Y} + e^{-\sqrt{D} \cdot z_Y}} \left( e^{\sqrt{D} \cdot z} - e^{-\sqrt{D} \cdot z} \right), & z_0 \leq z < z_Y \quad (11a) \\ E^{nt} \left[ \left( \frac{\sigma_z(z_Y)}{2E^{nt}} - \frac{B}{2\sqrt{A}} + \frac{\tau_Y \sqrt{A}}{2K_1} \right) e^{\sqrt{A}(z-z_Y)} - \left( -\frac{\sigma_z(z_Y)}{2E^{nt}} - \frac{B}{2\sqrt{A}} + \frac{\tau_Y \sqrt{A}}{2K_1} \right) e^{\sqrt{A}(z_Y-z)} \right], & z_Y \leq z \leq z_l \quad (11b) \end{cases}$$

$$\tau_i(z) = \begin{cases} \frac{K_1 u(z_Y)}{e^{\sqrt{D} \cdot z_Y} + e^{-\sqrt{D} \cdot z_Y}} \left( e^{\sqrt{D} \cdot z} + e^{-\sqrt{D} \cdot z} \right), & z_0 \leq z < z_Y \quad (12a) \\ K_2 \left[ \left( \frac{\sigma_z(z_Y)}{2E^{nt} \sqrt{A}} - \frac{B}{2A} + \frac{\tau_Y}{2K_1} \right) e^{\sqrt{A}(z-z_Y)} + \left( -\frac{\sigma_z(z_Y)}{2E^{nt} \sqrt{A}} - \frac{B}{2A} + \frac{\tau_Y}{2K_1} \right) e^{\sqrt{A}(z_Y-z)} + \frac{B}{A} - u(z_Y) \right] + \tau_Y, & z_Y \leq z \leq z_l \quad (12b) \end{cases}$$

Under relatively small stretching forces, the entire interfacial matrix layer may undergo purely elastic deformations. In this case, the solutions can be obtained by replacing  $u(z_Y)$  with  $u(z_l)$  in the elastic region solutions (Eqs. 11a and 12a) and are given as

$$\sigma_z(z) = \frac{\sqrt{D} E^{nt} u(z_l)}{e^{\sqrt{D} \cdot z_l} + e^{-\sqrt{D} \cdot z_l}} \left( e^{\sqrt{D} \cdot z} - e^{-\sqrt{D} \cdot z} \right), \quad z_0 \leq z \leq z_l, \tag{13}$$

$$\tau_i(z) = \frac{K_1 u(z_l)}{e^{\sqrt{D} \cdot z_l} + e^{-\sqrt{D} \cdot z_l}} \left( e^{\sqrt{D} \cdot z} + e^{-\sqrt{D} \cdot z} \right), \quad z_0 \leq z \leq z_l. \tag{14}$$

In the case of short embedded nanotube lengths, the entire interfacial matrix layer may undergo plastic deformations upon the crack initiation at the nanotube entry position. For this scenario, Eq. (1) can be simplified as

$$\tau_i = K_2 \cdot u(z), \quad z_0 \leq z \leq z_l \tag{15}$$

Consequently, by inserting Eq. (15) into Eq. (2), we can get

$$D_{nt} \cdot E^{nt} \frac{d^2 u(z)}{dz^2} - 4K_2 u(z) = 0, \quad z_0 \leq z \leq z_l. \tag{16}$$

The general solution of Eq. (16) is given as

$$u(z) = C_5 e^{\sqrt{A} \cdot z} + C_6 e^{-\sqrt{A} \cdot z}, \tag{17}$$

where  $C_5$  and  $C_6$  are two constants to be determined from the boundary conditions. The boundary conditions here are  $\sigma_z = 0$  at  $z = 0$  and  $u(z) = \frac{\tau_{max}}{K_2}$  at  $z = z_l$ , where  $\tau_{max}$  is the maximum interfacial shear strength between matrix and nanotube. Applying the boundary conditions to Eq. (17), we can get

$$C_5 = C_6 = \frac{u(z_l)}{e^{\sqrt{A} \cdot z_l} + e^{-\sqrt{A} \cdot z_l}}. \tag{18}$$

Substituting Eqs. (17) and (18) into Eqs. (1) and (3) leads to the solutions of the normal stress in the nanotube and the interfacial shear stress, which are given as

$$\sigma_z = \frac{E^{nt} u(z_l) \sqrt{A}}{e^{\sqrt{A} \cdot z_l} + e^{-\sqrt{A} \cdot z_l}} \left( e^{\sqrt{A} \cdot z} - e^{-\sqrt{A} \cdot z} \right), \quad z_0 \leq z \leq z_l, \tag{19}$$

$$\tau_i = \frac{K_2 u(z_l)}{e^{\sqrt{A} \cdot z_l} + e^{-\sqrt{A} \cdot z_l}} \left( e^{\sqrt{A} \cdot z} + e^{-\sqrt{A} \cdot z} \right), \quad z_0 \leq z \leq z_l. \tag{20}$$

It is noted that Gao et al. [28] reported an analytical solution on the IFSS distribution in fiber-reinforced nanocomposites by using the same single-fiber composite configuration as illustrated in Fig. 1a. In their work, both fiber and matrix are assumed to be purely elastic. By using the

notations in this work, the IFSS distribution reported in their work [28] is given as,

$$\tau_i = \frac{\alpha \sinh(\alpha z)}{4 \cosh(\alpha l)} \frac{(D_m^2 - D_{nt}^2) \left(1 - \frac{E^m}{E^{nt}}\right)}{D_{nt}^2 + \frac{E^m}{E^{nt}}(D_m^2 - D_{nt}^2)} \frac{P}{\pi D_{nt}}, \quad (21)$$

where  $\nu^m$  is the Poisson's ratio of matrix and  $\alpha$  is a parameter given as

$$\alpha^2 = \frac{1}{1 + \nu^m} \frac{D_m^2 - D_{nt}^2}{D_{nt}^2} \frac{D_{nt}^2 + \frac{E^m}{E^{nt}}(D_m^2 - D_{nt}^2)}{\frac{1}{4} D_m^4 \log \frac{D_m}{D_{nt}} - \frac{1}{16} (D_m^2 - D_{nt}^2)(3D_m^2 - D_{nt}^2)}. \quad (22)$$

When the interfacial matrix layer undergoes purely elastic deformation, the IFSS distribution given by Eq. (13) is considered to be identical to the solution given by Eq. (21). By comparing these two equations, we can get

$$K_1 = E^{nt} \frac{1}{1 + \nu^m} \frac{D_m^2 - D_{nt}^2}{D_{nt}^2} \frac{D_{nt}^2 + \frac{E^m}{E^{nt}}(D_m^2 - D_{nt}^2)}{D_m^4 \log \frac{D_m}{D_{nt}} - \frac{1}{4} (D_m^2 - D_{nt}^2)(3D_m^2 - D_{nt}^2)}. \quad (23)$$

The thickness of the interfacial matrix layer  $t$  is given as

$$t = \frac{G^m}{K_1} = \frac{E^m}{2E^{nt}} \frac{D_{nt}}{D_m^2 - D_{nt}^2} \frac{D_m^4 \log \frac{D_m}{D_{nt}} - \frac{1}{4} (D_m^2 - D_{nt}^2)(3D_m^2 - D_{nt}^2)}{D_{nt}^2 + \frac{E^m}{E^{nt}}(D_m^2 - D_{nt}^2)}. \quad (24)$$

Equations (23) and (24) show that both  $K_1$  and  $t$  depend only on the Young's moduli of nanotube and matrix as well as their diameters and are independent of the stretching force and the nanotube's embedded length. For the case that the diameter of the matrix is much larger than the diameter of the nanotube, i.e.,  $D_m \gg D_{nt}$ ,  $t$  can be simplified as

$$t \approx \frac{1}{2} \frac{E^m D_{nt} D_m^2}{E^{nt} D_{nt}^2 + E^m D_m^2} \left( \log \frac{D_m}{D_{nt}} - \frac{3}{4} \right). \quad (25)$$

With the known value of  $K_1$ , the complete IFSS and normal stress distribution profiles can be obtained from the closed-form analytical solutions derived above. In the following section, we employ the derived closed-form analytical solutions to quantify the interfacial load transfer characteristics on the nanotube–polymer interface based on our recently reported single-nanotube nanomechanical pull-out experiments [7, 19, 21].

### Quantification of the Interfacial Load Transfer on the Nanotube–Polymer Interface

Our recent nanomechanical single-nanotube pull-out experiments quantify the interfacial load transfer characteristics of the respective interfaces formed between individual CNTs or BNNTs and PMMA or epoxy polymers [7, 19, 21]. The

CNTs employed in the single-nanotube pull-out measurements, which were synthesized using chemical vapored deposition methods, are double-walled nanotubes with a polydispersed diameter within the range of 2.0–4.2 nm and a median diameter of 3.1 nm. The employed BNNTs were synthesized using high temperature pressured methods and were found to be mostly single- to quadruple-walled [41, 42]. Double-walled BNNTs reportedly have a dominant presence (> 57%) with diameters within the range of 1.9–3.9 nm and a median diameter of 2.9 nm [43]. The employed PMMA polymer has a molecular weight of 50,000. The epoxy polymer is Epon 828 difunctional bisphenol A/epichlorohydrin epoxy resin with curing agent EPIKURE 3200 aminoethylpiperazine (AEP). It is noted that the present theoretical prediction are conducted by using the same set of material and geometry parameters as employed in our prior work [7, 19, 21], which are listed in Table 1.

### The Dependence of the Interfacial Shear Stress on the Stretching Force

Here we investigate the evolution of the IFSS on the nanotube–polymer interface under an increasing stretching force  $P$  using the closed-form solutions derived above. For illustration and discussion, we study the load transfer characteristics of a CNT–PMMA interface. CNT is considered as an elastic material with a Young's modulus  $E^{nt} = 1.0\text{TPa}$ . PMMA is assumed as a bilinear strain-hardening material with a Young's modulus  $E^m = 1.74\text{GPa}$ , a Poisson's ratio  $\nu^m = 0.32$ , a tangent modulus after yielding  $E_p^m = 105\text{MPa}$ , a yield stress of 81 MPa and a corresponding yield shear stress  $\tau_y = 46.7\text{MPa}$  [33], and calculated shear modulus  $G^m = 0.66\text{GPa}$  (before yielding) and  $G_p^m = 35\text{MPa}$  (after yielding). The theoretical predications are calculated based on the following parameters: a matrix diameter  $D_m = 1.6\ \mu\text{m}$ , a CNT with a diameter of 3.1 nm and an embedded length  $l = 800\text{ nm}$ , and a pull-out force  $P_{out} = 157.6\text{ nN}$  (an experimental value [19]). Coefficients  $K_1$  and  $K_2$  are calculated to be  $K_1 = 7.76 \times 10^{16}\text{ N/m}^3$ , and  $K_2 = 4.15 \times 10^{15}\text{ N/m}^3$  by using Eq. (23). The thickness of the interfacial matrix layer  $t$  is found to be about 8.50 nm. All of these employed and calculated parameters are listed in Table 1.

Figure 2a shows three selected and representative IFSS distribution profiles on the CNT–PMMA interface up to the pull-out event and Fig. 2b shows the dependence of the maximum IFSS,  $\tau_{max}$ , is found to be about 10.3 MPa, below the matrix's yield strength (46.7 MPa). The entire interfacial matrix layer undergoes purely elastic deformations. When the force increase to 45.5 nN,  $\tau_{max}$  reaches the matrix's yield shear strength, indicating the onset of yield deformations in the matrix at the nanotube's entry position. The matrix near the nanotube entry position begins to undergo plastic

**Table 1** The summary of the parameters used to predict the interfacial load transfer on four types of nanotube–polymer interfaces and some of the calculated parameters using the present strain-hardening

shear-lag model and the comparison with the values obtained using the elastic shear-lag model

Interface type	CNT–PMMA	CNT–epoxy	BNNT–PMMA	BNNT–epoxy
Young's modulus of polymer	PMMA: 1.74 GPa [32]; epoxy: 2.8 GPa [39]			
Tangent modulus of polymer	PMMA: 0.105 GPa [32]; epoxy: 0.41 GPa [39]			
Poisson's ratio of polymer	PMMA: 0.32 [32]; epoxy: 0.33 [39]			
Yield shear strength of polymer	PMMA: 46.7 MPa [32]; epoxy: 20 MPa [39]			
Young's modulus of nanotubes	CNT: 1000 GPa [21]; BNNT: 1070 GPa [7]			
Median Diameter of nanotubes	CNT: 3.1 nm [21]; BNNT: 2.9 nm [7]			
Diameter of polymer	PMMA: 1.6 $\mu\text{m}$ [7, 19]; epoxy: 2.0 $\mu\text{m}$ [7, 21]			
Coefficients $K_1$ (N/m <sup>3</sup> )	$7.76 \times 10^{16}$	$11.9 \times 10^{16}$	$8.19 \times 10^{16}$	$12.6 \times 10^{16}$
Coefficients $K_2$ (N/m <sup>3</sup> )	$0.415 \times 10^{16}$	$1.57 \times 10^{16}$	$0.438 \times 10^{16}$	$1.66 \times 10^{16}$
Thickness of interface matrix layer $t$ (nm)	8.50	8.86	8.05	8.38
Pull-out load in the force plateau (nN)	$158 \pm 14$ [19]	$226 \pm 11$ [21]	$193 \pm 10$ [7]	$246 \pm 16$ [7]
Critical embedded nanotube length (nm)	366	482	386	483
Maximum IFSS (MPa)				
Present strain-hardening shear-lag model	$59 \pm 2$	$106 \pm 5$	$71 \pm 2$	$133 \pm 9$
Elastic shear-lag model [28]	$162 \pm 14$	$287 \pm 14$	$236 \pm 11$	$361 \pm 24$

The numbers in the brackets refer to the reference numbers

deformations and the plastic deformation region expands under an increasing stretching force. When the stretching force reaches the pull-out value ( $P_{out} = 157.6$  nN), the plastic deformation region is found to have a length of about 223 nm, while the elastic deformation region has a length of about 577 nm.  $\tau_{max}$  is found to be about 59 MPa. In comparison, by assuming that the matrix is a purely elastic material,  $\tau_{max}$  is calculated to be about 162 MPa by using the shear-lag model reported in Ref. [28] or about 163 MPa by using a similar shear-lag model reported in Ref. [30]. Therefore, the calculated maximum IFSS based on the strain-hardening model is substantially lower than the values predicted using the elastic models.

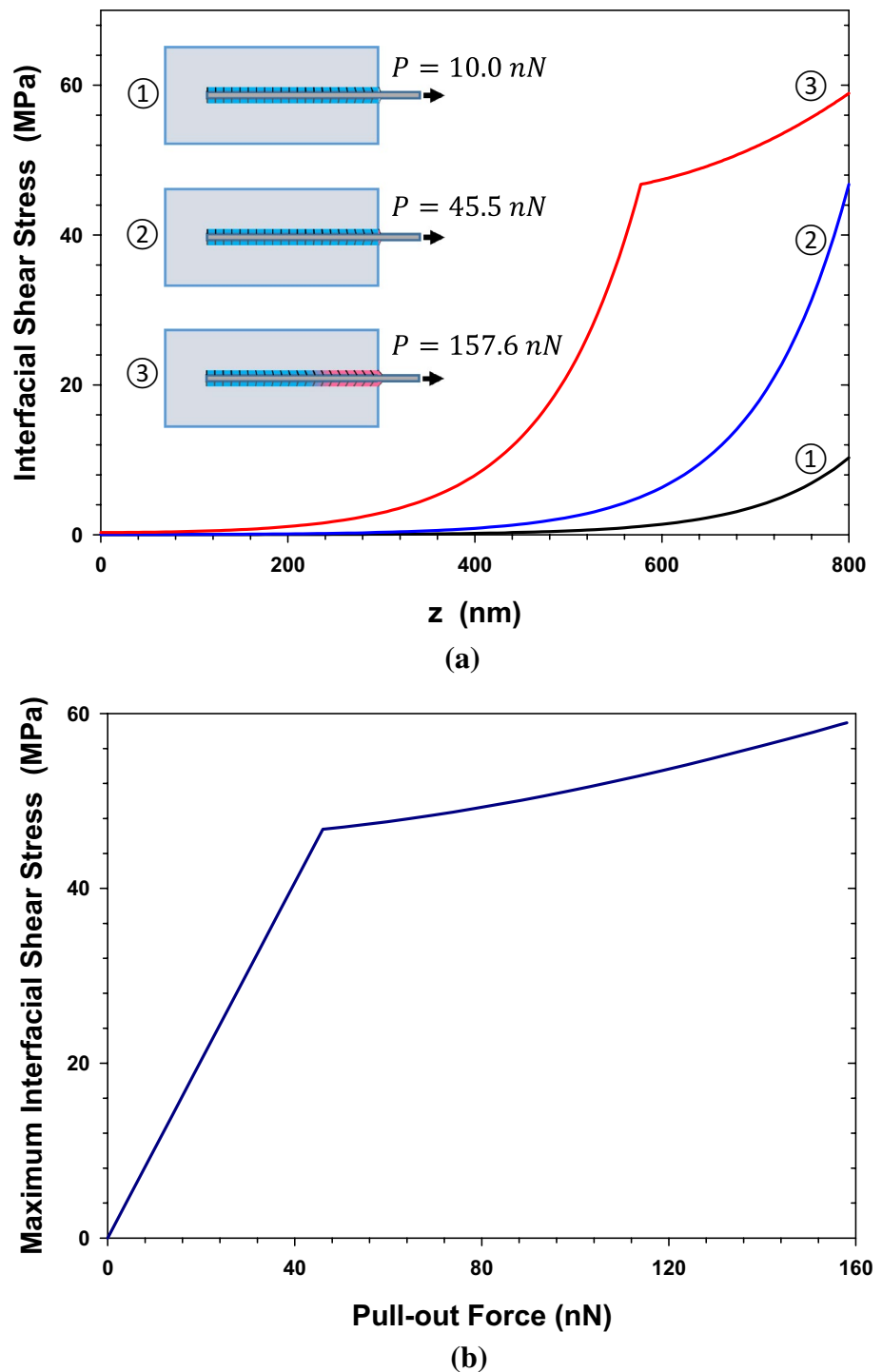
### The Dependence of the Interfacial Shear Stress on the Embedded Nanotube Length

The embedded nanotube length is expected to have a substantial influence on the IFSS distribution profile. It has been demonstrated in prior single-nanotube pull-out experiments that the pull-out force initially increases with the embedded nanotube length and then reaches a plateau once the embedded nanotube length exceeds a critical threshold value. Here, we investigate the dependence of the IFSS distribution profile on the embedded nanotube length. The plots in Fig. 3 show the IFSS profiles of the CNT–PMMA interfaces with five selected embedded nanotube lengths at the moment of pull-out: (a)  $l = 200$  nm and the corresponding applied pull-out force  $P_{out} = 107.2$  nN; (b)  $l = 400$  nm and  $P_{out} = 156.9$  nN; (c)  $l = 600$  nm and  $P_{out} = 157.5$  nN;

(d)  $l = 800$  nm and  $P_{out} = 157.6$  nN; (e)  $l = 1000$  nm and  $P_{out} = 157.6$  nN. The employed pull-out force values for  $l \geq 800$  nm are set based on our prior pull-out measurements on the CNT–PMMA interface [19], while the employed pull-out force values for  $l \leq 600$  nm are theoretically predicted based on the same calculated maximum interfacial shear stress of the CNT–PMMA interface, which is found to be about 59 MPa. For  $l = 200$  nm, the IFSS profile displays only one segment and its value is found to be within the range of 53–59 MPa and is higher than the matrix's yield shear stress. This result indicates that the entire interfacial matrix layer undergoes plastic deformations. For  $l = 400$  nm, the IFSS profile displays two segments: an elastic zone (for  $z < 173$  nm) and a plastic zone (for  $173 \text{ nm} \leq z \leq 400$  nm). The IFSS at the nanotube's embedded end is found to be about 16 MPa. A similar IFSS distribution profile is exhibited for the case of  $l = 600$  nm with a larger elastic zone (about 378 nm in length), a similar-size plastic zone (about 222 nm in length), and a lower IFSS at the nanotube's embedded end (about 2 MPa) as compared to the one for  $l = 400$  nm. For  $l = 800$  nm, its plastic zone is found to be identical to the one in the case of  $l = 600$  nm. It is noticed that the IFSS approaches zero at the nanotube's embedded end. This observation indicates that the total load transferred via the nanotube–polymer interface, which is represented by the area under the IFSS curve, reaches its maximum value. This finding is further corroborated by the curve obtained for  $l = 1000$  nm, which displays an identical plastic zone and an elastic zone with a similar trend as for  $l = 800$  nm. The findings here indicate that the interfacial matrix layer upon



**Fig. 2** **a** Selected representative interfacial shear stress distribution profiles of a CNT–PMMA interface with an embedded nanotube length of 800 nm under three different stretching forces: (1) 10 nN; (2) 45.5 nN; (3) 157.6 nN. **b** The dependence of the maximum interfacial shear stress on the pull-out force



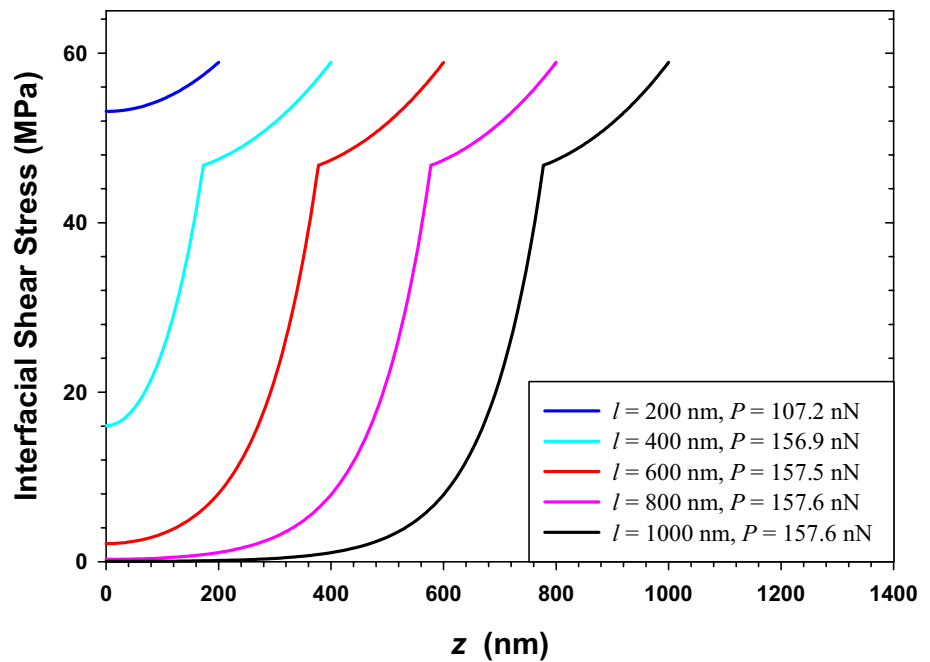
the occurrence of pull-out event deforms either in a purely plastic or a mixed elastic–plastic manner, which depends on the embedded nanotube length. Our analysis further reveals that the embedded nanotube length at which the deformation mechanism transition occurs is found to be about 305 nm for the examined CNT–PMMA interface. Therefore, it is of importance to take into account the strain-hardening properties of the matrix in the theoretical analysis of the

interfacial stress transfer characteristics of nanotube–polymer interfaces.

#### Comparison of the IFSS distribution profiles across different nanotube–polymer interfaces

Figure 4a–d show the calculated IFSS distribution profiles corresponding to the occurrence of pull-out (i.e.,  $P = P_{out}$ ) for four

**Fig. 3** Selected representative interfacial shear stress distribution profiles of CNT–PMMA interfaces with different embedded nanotube lengths at the moment of pull-out



types of nanotube–polymer interfaces that were characterized by single-nanotube pull-out experiments [7, 19, 21]. The blue curves are calculated by using the strain-hardening shear-lag model as presented in this work, while the red curves are calculated by using the elastic shear-lag model that is given by Eq. (21). All of the calculations are based on the same embedded nanotube length (800 nm) and the respectively measured average pull-out forces in the plateau region. All of the other employed parameters in the calculations and the calculated relevant parameters, including the calculated values of the maximum IFSS, are listed in Table 1.

As displayed in Fig. 4a–d, the strain-hardening model consistently predicts a much lower maximum IFSS, as compared with the elastic model. For example, for the BNNT–PMMA interface, the maximum IFSS is found to be about 71 MPa by using the strain-hardening model, which is less than one-third of the value predicted by using the elastic model (about 236 MPa). The results also show that the BNNT–epoxy interface that possesses a maximum IFSS of 133 MPa is the strongest among the four types of nanotube–polymer interfaces, while the CNT–PMMA interface is the weakest one with a maximum IFSS of about 59 MPa. It is noticed that both models predict the same ranking of the interfacial strength among these four types of nanotube–polymer interfaces.

### The Dependence of the Pull-Out Force on the Embedded Nanotube Length

Figure 5a–d show the theoretically predicted relationships between the pull-out force and the embedded nanotube

length for the four types of nanotube–polymer interfaces by using the strain-hardening shear-lag model and their comparison with the respective measurement data [7, 19, 21]. It can be seen that the theoretical predictions are generally in good agreement with the experimental measurements. Relatively large discrepancies are exhibited for those pull-out data with short embedded nanotube lengths, for which the corresponding pull-out load is in an increasing trend. The observed discrepancies can be attributed to several sources. The first and probably the most significant one is that the diameters of the nanotubes employed in the experiments are polydispersed, while the theoretical calculations are based on the measured median nanotube diameter. Other factors include the measurement uncertainties of the pull-out force and the embedded nanotube length, which may become more significant for relatively short embedded nanotube lengths and relatively low pull-out forces. By considering the scattering of the measured pull-out force in the plateau region, the maximum IFSS is calculated by using the strain-hardening and elastic shear-lag models and the results are listed in Table 1. For example, the BNNT–PMMA interface is found to possess a maximum IFSS of  $71 \pm 2$  MPa that is predicted using the strain-hardening model, as compared to  $236 \pm 11$  MPa that is predicted using the elastic model.

The critical embedded nanotube length is an important parameter in the load transfer characteristic of the nanotube–polymer interface. However, the quantification of its value varies depending on the determination criterion of where the force plateau initiates in the pull-out force versus the embedded nanotube length curve. Here we quantify the critical embedded length by assuming that it corresponds

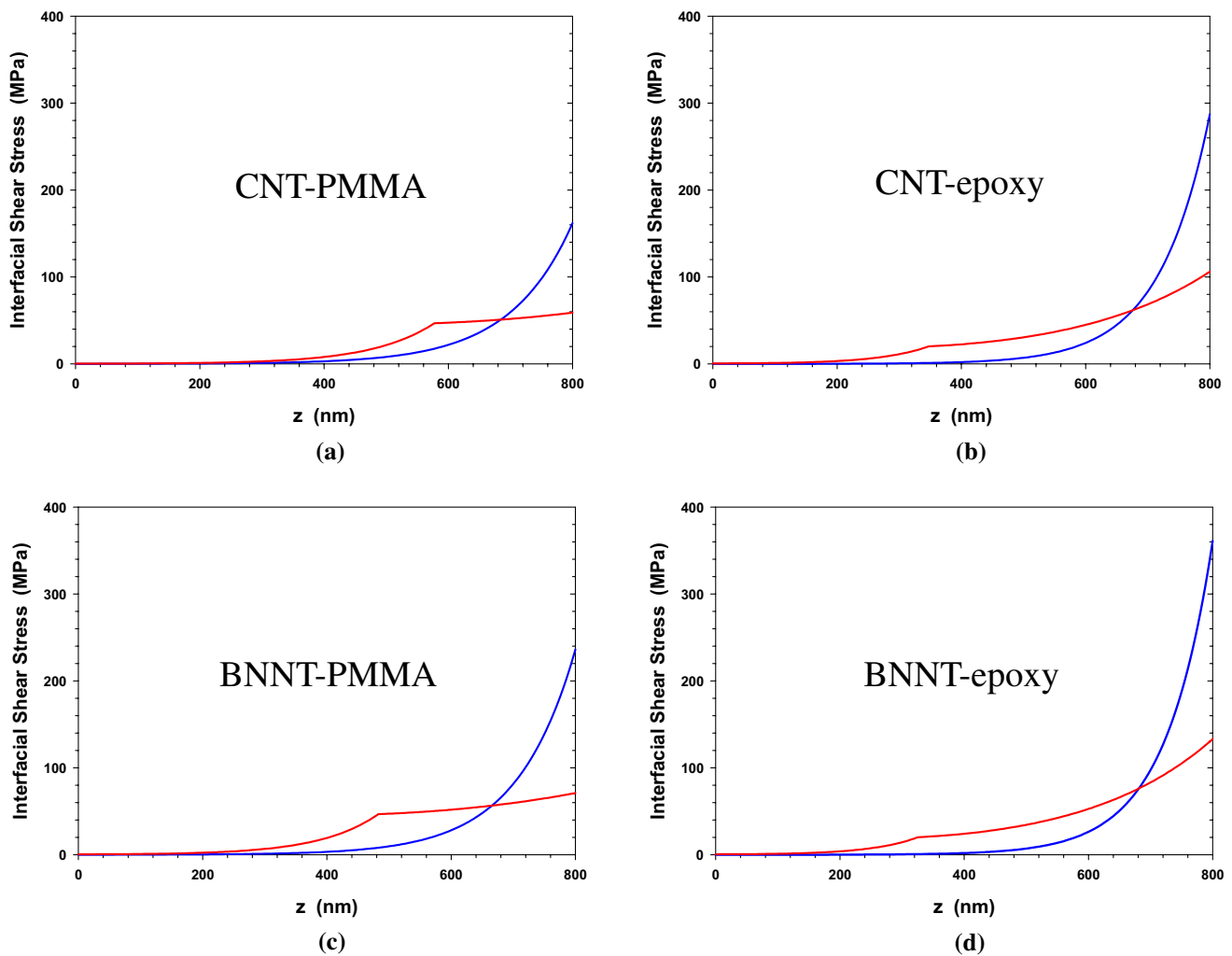


**Fig. 4** Comparison of the theoretically predicted IFSS distribution profiles for **a** CNT–PMMA; **b** CNT–epoxy; **c** BNNT–PMMA; **d** BNNT–epoxy interfaces by using the strain-hardening shear-lag model (red curves) and the elastic shear-lag model (blue curve). All

of the calculations are based on the same embedded nanotube length (800 nm) and the respectively measured average pull-out forces in the plateau region

to a pull-out force that is 1% below the average force in the plateau region. The critical embedded length for the CNT–PMMA interface is found to be about 366 nm, while about 482 nm for the CNT–epoxy interface, about 386 nm for the BNNT–PMMA interface, and about 483 nm for the BNNT–epoxy interface.

## Conclusion

In this paper, we investigate the interfacial shear transfer characteristics of nanotube-reinforced polymer nanocomposites by using a strain-hardening shear-lag model. The proposed model and the derived closed-form analytical solutions are shown to be capable of predicting the IFSS distribution profile on the nanotube–polymer interface more

realistically and accurately as compared to prior work by using elastic shear-lag models. The theoretical analysis captures the dependence of the pull-out force on the embedded nanotube length by identifying the mechanical deformations of the interfacial matrix layer, which is shown to be in good agreement with experimental measurements. The results contribute to a complete understanding of the interfacial load transfer in nanofiber-reinforced polymer nanocomposites and ultimately contribute to the optimal design and performance of lightweight and high-strength nanocomposite materials. The derived closed-form analytical solutions can be extended to the study of the interfacial load transfer in 1D nanofiber-reinforced metal and ceramic composites, such as our recent work on carbon nanotube metal interfaces [44, 45] and boron nitride ceramic interfaces [46]. By considering that nanotubes are the rollups of 2D materials, such as

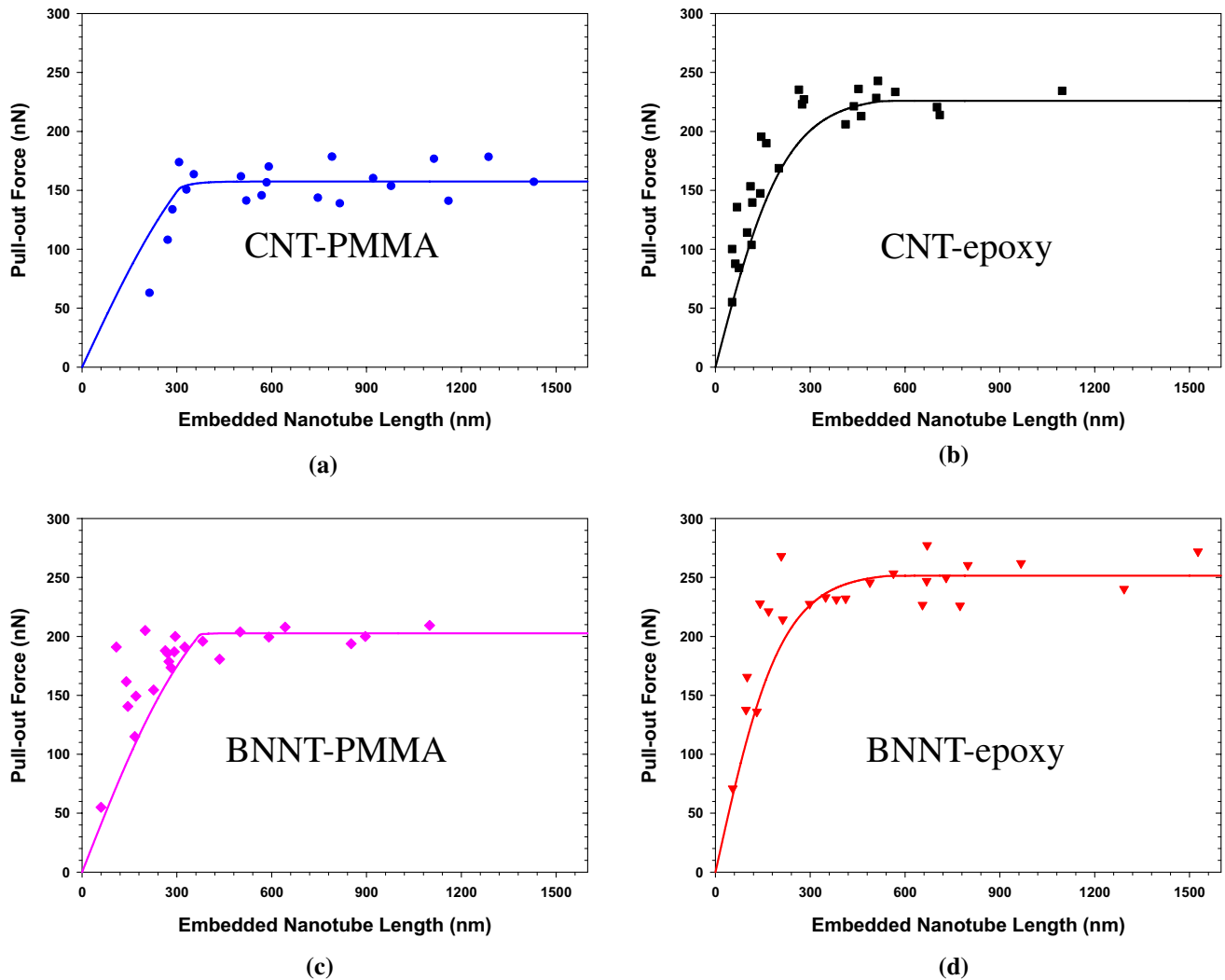


**Fig. 5** The comparison of the theoretically predicted pull-out force versus the embedded nanotube length profiles (solid curves) with experimental measurements (dots) for **a** CNT–PMMA; **b** CNT–

epoxy; **c** BNNT–PMMA; **d** BNNT–epoxy interfaces. The experimental measurement data are reproduced from Refs. [7, 19, 21]

graphene and thin h-BN, the derived analytical solutions can be also adapted to the study of the interfacial load transfer in 2D material based composites and devices, such as our recent work on the thermal-induced mechanical deformation of ultrathin h-BN on silicon dioxide substrates [47].

**Acknowledgements** This work was supported by the US Air Force Office of Scientific Research—Low Density Materials program under Grant no. FA9550-15-1-0491, and by National Science Foundation under Grant no. CMMI-1537333.

## References

1. S. Iijima, *Nature* **354**, 56 (1991)
2. A. Rubio, J.L. Corkill, M.L. Cohen, *Phys. Rev. B* **49**, 5081 (1994)
3. N.G. Chopra, R.J. Luyken, K. Cherrey, V.H. Crespi, M.L. Cohen, S.G. Louie, A. Zettl, *Science* **269**, 966 (1995)
4. M. Moniruzzaman, K.I. Winey, *Macromolecules* **39**, 5194 (2006)
5. Q. Cheng, B. Wang, C. Zhang, Z. Liang, *Small* **6**, 763 (2010)
6. C. Zhi, Y. Bando, T. Terao, C. Tang, H. Kuwahara, D. Golberg, *Adv. Funct. Mater.* **19**, 1857 (2009)
7. X. Chen, L. Zhang, C. Park, C.C. Fay, X. Wang, C. Ke, *Appl. Phys. Lett.* **107**, 253105 (2015)
8. M.L. Minus, H.G. Chae, S. Kumar, *Polymer* **47**, 3705 (2006)
9. Y. Zhang, K. Song, J. Meng, M.L. Minus, *A.C.S. Appl. Mater. Interfaces* **5**, 807 (2013)
10. X. Tao, L. Dong, X. Wang, W. Zhang, B.J. Nelson, X. Li, *Adv. Mater.* **22**, 2055 (2010)
11. H.D. Wagner, O. Lourie, Y. Feldman, R. Tenne, *Appl. Phys. Lett.* **72**, 188 (1998)
12. C.A. Cooper, S.R. Cohen, A.H. Barber, H.D. Wagner, *Appl. Phys. Lett.* **81**, 3873 (2002)

13. A.H. Barber, S.R. Cohen, H.D. Wagner, *Appl. Phys. Lett.* **82**, 4140 (2003)
14. A.H. Barber, S.R. Cohen, S. Kenig, H.D. Wagner, *Compos. Sci. Technol.* **64**, 2283 (2004)
15. A.H. Barber, S.R. Cohen, A. Eitan, L.S. Schadler, H.D. Wagner, *Adv. Mater.* **18**, 83 (2006)
16. M.P. Manoharan, A. Sharma, A.V. Desai, M.A. Haque, C.E. Bakis, K.W. Wang, *Nanotechnology* **20**, 295701 (2009)
17. T. Tsuda, T. Ogasawara, F. Deng, N. Takeda, *Compos. Sci. Technol.* **71**, 1295 (2011)
18. Y. Ganesan, C. Peng, Y. Lu, P.E. Loya, P. Moloney, E. Barrera, B.I. Yakobson, J.M. Tour, R. Ballarini, J. Lou, *ACS Appl. Mater. Interfaces.* **3**, 129 (2011)
19. X. Chen, M. Zheng, C. Park, C. Ke, *Small* **9**, 3345 (2013)
20. Y. Ganesan, H. Salahshoor, C. Peng, V. Khabashesku, J. Zhang, A. Cate, N. Rahbar, J. Lou, *J. Appl. Phys.* **115**, 224305 (2014)
21. X. Chen, L. Zhang, M. Zheng, C. Park, X. Wang, C. Ke, *Carbon* **82**, 214 (2015)
22. B.A. Newcomb, H.G. Chae, P.V. Gulgunje, K. Gupta, Y. Liu, D.E. Tsentalovich, M. Pasquali, S. Kumar, *Polymer* **55**, 2734 (2014)
23. D. Roy, S. Bhattacharyya, A. Rachamim, A. Plati, M.-L. Saboungi, *J. Appl. Phys.* **107**, 043501 (2010)
24. B. Soumendu, H. Abhilash, C.H. Beng, *Proc. R. Soc. Math. Phys. Eng. Sci.* **474**, 20170705 (2018)
25. H.L. Cox, *Br. J. Appl. Phys.* **3**, 72 (1952)
26. C.-H. Hsueh, *Mater. Sci. Eng. A* **125**, 67 (1990)
27. C.-H. Hsueh, *Mater. Sci. Eng. A* **154**, 125 (1992)
28. X.-L. Gao, K. Li, *Int. J. Solids Struct.* **42**, 1649 (2005)
29. C.M. Landis, R.M. McMeeking, *Compos. Sci. Technol.* **59**, 447 (1999)
30. K.R. Jiang, L.S. Penn, *Compos. Sci. Technol.* **45**, 89 (1992)
31. T. Ozkan, Q. Chen, I. Chasiotis, *Compos. Sci. Technol.* **72**, 965 (2012)
32. P. Moy, C.A. Gunnarsson, T. Weerasooriya, W. Chen, *Dynamic Behavior of Material*, vol. 1 (Springer, New York, 2011), pp. 125–133
33. R.E. Gorga, R.E. Cohen, *J. Polym. Sci. Part B Polym. Phys.* **42**, 2690 (2004)
34. E.T. Kopesky, G.H. McKinley, R.E. Cohen, *Polymer* **47**, 299 (2006)
35. V. Sankar, T.S. Kumar, K.P. Rao, *Trends Biomater Artif Organs* **17**(2), 24 (2004)
36. F. Povolò, É.B. Hermida, *J. Appl. Polym. Sci.* **58**, 55 (1995)
37. M. Nasraoui, P. Forquin, L. Siad, A. Rusinek, *Mater. Des.* **37**, 500 (2012)
38. D. Rittel, N. Eliash, J.L. Halary, *Polymer* **44**, 2817 (2003)
39. Epon Resin Structural Reference Manual, *Epon Resin Structural Reference Manual* (Resolution Performance Products LLC, 2001)
40. W.-F. Chen, D.J. Han, *Plasticity for Structural Engineers* (J. Ross Publishing, Fort Lauderdale, 2007)
41. M.W. Smith, K.C. Jordan, C. Park, J.-W. Kim, P.T. Lillehei, R. Crooks, J.S. Harrison, *Nanotechnology* **20**, 505604 (2009)
42. M. Zheng, C. Ke, I.-T. Bae, C. Park, M.W. Smith, K. Jordan, *Nanotechnology* **23**, 095703 (2012)
43. V. Yamakov, C. Park, J.H. Kang, X. Chen, C. Ke, C. Fay, *Comput. Mater. Sci.* **135**, 29 (2017)
44. C. Yi, X. Chen, F. Gou, C.M. Dmuchowski, A. Sharma, C. Park, C. Ke, *Carbon* **125**, 93 (2017)
45. C. Yi, S. Bagchi, C.M. Dmuchowski, F. Gou, X. Chen, C. Park, H.B. Chew, C. Ke, *Carbon* **132**, 548 (2018)
46. C. Yi, S. Bagchi, F. Gou, C.M. Dmuchowski, C. Park, C.C. Fay, H.B. Chew, C. Ke, *Nanotechnology* **30**, 025706 (2019)
47. W. Qu, F. Gou, C. Ke, *Appl. Phys. Lett.* **114**, 051901 (2019)

**Publisher's Note** Springer Nature remains neutral with regard to jurisdictional claims in published maps and institutional affiliations.